State-to-state photodissociation of OCS($\nu_2=0,1|JIM$). I. The angular recoil distribution of CO($X^1\Sigma^+; v=0|J$)

Alrik J. van den Brom
Laser Centre and Department of Chemistry, Vrije Universiteit, de Boelelaan 1083, 1081 HV Amsterdam, The Netherlands

T. Peter Rakitzis
Department of Physics, University of Crete, and IESL-FORTH, P.O. Box 1527, 71110, Heraklion, Greece

Jeroen van Heyst
Laser Centre and Department of Chemistry, Vrije Universiteit, de Boelelaan 1083, 1081 HV Amsterdam, The Netherlands

Theofanis N. Kitsopoulos
Department of Chemistry, University of Crete, and IESL-FORTH, P.O. Box 1527, 71110, Heraklion, Greece

Sebastian R. Jezowski[a]
Faculty of Chemistry, Wroclaw University, 14 F. Joliot-Curie, 50-383 Wroclaw, Poland

Maurice H. M. Janssen[b]
Laser Centre and Department of Chemistry, Vrije Universiteit, de Boelelaan 1083, 1081 HV Amsterdam, The Netherlands

State-to-state photodissociation experiments of OCS at 230 nm are reported using hexapole state selection of the parent molecule and velocity map ion imaging of the angular recoil of the CO photofragment. The role of the initial rovibrational state ($\nu_2=0,1|JlM$) of OCS on the angular recoil distribution is investigated. The CO($X^1\Sigma^+; v=0|J$) rotational distribution as well as the angular recoil anisotropy parameter β of the CO photofragment are reported for dissociation of single rovibrational ($\nu_2=0,1|JlM$) quantum states of OCS. A strong dependence of the anisotropy parameter β on the initial bending state, $\nu_2=0$ or 1, of OCS is observed. The effects of the initial bending state of OCS are rationalized in terms of the strong angular dependence of the transition dipole moment function of OCS for the $1\,^1\Sigma^-(1\,^1A'')$ and $1\,^1\Delta(2\,^1A')$ excited state surfaces involved in the dissociation at 230 nm. The state-to-state imaging experiment provides a revised and improved determination of the binding energy of OCS($\nu_1,\nu_2,\nu_3=0,0,0|J=0$)$\rightarrow$CO($X^1\Sigma^+; v=0|J=0$)$+$S($^1D_2$), $D_0=(4.284\pm0.009)$ eV. © *2002 American Institute of Physics.*
[DOI: 10.1063/1.1496464]

I. INTRODUCTION

During recent years progress in experimental techniques is advancing photodissociation studies to the level of complete quantum state-to-state unimolecular scattering with angular-resolved detection of photofragments.[1,2] The formation of electronically excited atomic photofragments has attracted strong interest, as the anisotropy of the magnetic sublevels of the electronic orbital provides detailed information on the photodynamics, the multiple potential energy surfaces accessed, and nonadiabatic processes during the dissociation. Time-of-flight and ion-imaging experiments have been reported on the photodissociation of the diatomic molecules ICl, Cl$_2$,[3-6] O$_2$,[7] and the triatomic molecules N$_2$O,[8-10] OCS[11-14] and O$_3$.[15] In the above experiments cold molecular

beams were used, which means that under favorable conditions only a few rotational states are populated and contribute to the measured observables. In a few cases single quantum states of the parent molecule were selected either through a laser selective multiphoton preparation scheme[7] or hexapole state selectors.[2,9,16] For the triatomic benchmark molecules N$_2$O and OCS it is known that in the first dissociation bands the dynamics is not only from the vibrationless ground state but also from vibrationally excited states. Especially the low lying bending states contribute to the dissociation in the red part of the absorption band.[9,17] It has been shown that the dissociation from excited bending states may explain the observed anomalies in the isotopomer distribution of N$_2$O in the stratosphere.[18]

When studying the photodissociation dynamics of a molecule, the energetic aspects (electronic, vibrational, rotational, translational) as well as the spatial distribution of the nascent fragments are to be considered. The spatial recoil distribution of fragments can be described by the anisotropy

---

[a] Present address: Huygens Laboratory, Leiden University, P.O. Box 9504, 2300 RA Leiden, The Netherlands.
[b] Author to whom correspondence should be addressed. Electronic mail: mhmj@chem.vu.nl

parameter β, which reflects the dissociation dynamics and the symmetry of the potential energy surfaces (PES) involved. The β parameter is defined as

$$I(\theta) = \frac{\sigma}{4\pi}[1 + \beta P_2(\cos\theta)], \qquad (1)$$

where θ is the laboratory frame angle between the linear polarization of the dissociation laser and the recoil velocity of the photofragment, and $P_2(\cos\theta)$ the second-order Legendre polynomial.

Very recently, it was shown how the alignment of the $S(^1D_2)$ photofragment can be measured completely using Abel-invertible ion images employing various pump–probe polarization geometries.[14,19] Experimentally, the $S(^1D_2)$ or $CO(X\,^1\Sigma^+;J)$ photofragments are detected using a $(2+1)$ resonance-enhanced multiphoton ionization (REMPI) scheme. For an isotropic ensemble of parent molecules, the angular distribution can then be expressed in an expansion of orthogonal Legendre polynomials:[19]

$$I(\theta) = 1 + \beta_2 P_2(\cos\theta) + \beta_4 P_4(\cos\theta) + \beta_6 P_6(\cos\theta). \qquad (2)$$

The parameters β_2, β_4, and β_6 contain information on both the conventional recoil anisotropy parameter β [Eq. (1)] as well as the alignment of the electronic angular momentum of the $S(^1D_2)$ state. For the $CO(X\,^1\Sigma^+;J)$ fragment and $(2+1)$ REMPI via the Q band of the $B\,^1\Sigma^+$ state, the detection scheme is not sensitive to the photofragment alignment,[20] and the β_4 and β_6 coefficients in Eq. (2) vanish. When the axial recoil approximation applies, an intermediate value of β ($-1 < \beta < 2$) indicates that two or more potential surfaces are coherently excited, or the transition dipole moment of the transition from the ground state to the excited state is neither purely parallel ($\beta = 2.0$) nor perpendicular ($\beta = -1.0$).[19]

The linear molecule OCS is a 16 valence electron system, which, like N_2O, CS_2, and CO_2, is bent in the low lying dissociative excited states. Therefore, a strong torque is exerted on the CO fragment during the dissociation, and the released CO is highly rotationally excited.[11,21,22] For the bent molecule the symmetry of the linear OCS molecule ($C_{\infty v}$) is lowered to C_s. The ground state is of A' symmetry, and the $1\,^1\Delta$ excited state splits into the $2\,^1A'$ and $2\,^1A''$ states. The nearby $1\,^1\Sigma^-$ state correlates with the $1\,^1A''$ state. Suzuki and co-workers reported[11] that dynamics on the $2\,^1A'$ and $1\,^1A''$ surfaces combined with nonadiabatic transitions between the excited $2\,^1A'$ surface and the ground state $1\,^1A'$ surface, were responsible for a bimodal rotational distribution of $CO(X\,^1\Sigma^+;J)$. The potential energy surfaces as a function of bond angle are schematically drawn in Fig. 1. The nonadiabatic transitions to the $1\,^1A'$ ground state produce predominantly translationally slow CO fragments in high-J states ($J \approx 63$), whereas fast CO fragments in lower-J states ($J \approx 51$) result from the dissociation on both $2\,^1A'$ and $1\,^1A''$ surfaces.[11]

Differences in the spatial anisotropy have been reported for the slow and fast channel.[17,20] The $2\,^1A'$ excited surface is accessed through a parallel transition, while the $1\,^1A''$ ex-
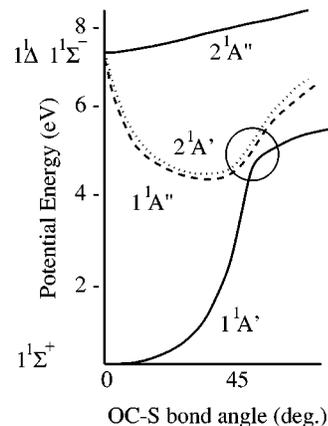

FIG. 1. Schematic picture of the OCS potential energy surfaces as a function of the OC–S bond angle at an equilibrium distance. Along the potential energy axis, the symmetry species of the PES of linear OCS are denoted. The circle indicates the area where nonadiabatic interaction between the $2\,^1A'$ and $1\,^1A'$ can occur. Adapted from Refs. 11, 17.

cited surface is accessed through a perpendicular transition. The transition dipole moment of each of these surfaces varies strongly with the OC–S bond angle.[11]

In this paper we report measurements of the state-to-state photolysis of OCS at 230 nm. To assess the effect of the initial rovibrational quantum state on the photodynamics of OCS, a hexapole state selector is used to prepare the parent molecule in a single rovibrational quantum state.[2] OCS is a linear molecule in the vibrational ground state $(\nu_1, \nu_2, \nu_3) = (0,0,0)$ and the $(JM) = (10)$ state can be focused due to the second-order Stark effect.[23] OCS in the vibrationally excited state $(\nu_1, \nu_2, \nu_3) = (0,1^1,0)$, can be focused using the first-order Stark effect. A linear molecule in the $(0,1^1,0)$ bending mode behaves like a symmetric top (JlM) molecule with angular momentum J, projecting $l = 1$ along the symmetry axis.[24,25] The hexapole focusing conditions for first-order and second-order Stark effect are different and by choosing the appropriate carrier gas we have separated the $(\nu_2 = 0 | JM = 10)$ and $(\nu_2 = 1 | JlM = 111)$ states.

In Sec. II we give a short description of the experimental setup. In Sec. III we present the rotational state distribution of CO and the angular recoil disitribution for selected initial rovibrational quantum states of OCS. In Sec. IV we discuss the results and compare with theoretical calculations. Finally, in Sec. V we will summarize our conclusions.

II. EXPERIMENT

The hexapole-imaging apparatus has been described in detail before.[2] The ion optics with grids used in the first generation of hexapole-imaging experiments[2,9,16] were replaced for the current experiments by a new velocity-map ion lens setup, following the design reported by Eppink and Parker.[26] A 20% mixture of OCS in Ar is supersonically expanded via a pulsed nozzle and skimmed before it enters the second differentially pumped chamber. In this second chamber a beamstop (a small metal sphere of diameter 1.5 mm, which can be translated under vacuum) is positioned on the beam axis, 20 cm downstream of the nozzle and 10 cm upstream of the entrance of the hexapole field. The center of the

J. Chem. Phys., Vol. 117, No. 9, 1 September 2002
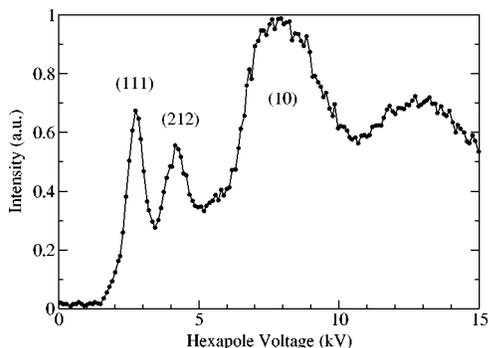
Photodissociation of OCS   4257

FIG. 2. Hexapole focusing spectrum of OCS (20% in Ar). The hexapole voltage equals the total potential difference across the positive and negative rods. The assigned (JlM) rotational states are denoted. At voltages above 10 kV, second-order focusing occurs. For brevity, the OCS $(\nu_2=1|JlM=111)$, $(\nu_2=1|JlM=212)$, and $(\nu_2=0|JM=10)$ states are indicated as (111), (212), and (10), respectively.

molecular beam hits the beamstop preventing molecules in non- or weakly focusable states from reaching the laser interaction region. The molecules in positive Stark-effect states, which expand through the first skimmer within the solid angle determined by the hexapole geometry[27,28] and pass the beamstop, enter the third chamber where they are focused by the hexapole field onto a small collimator (diameter 1.5 mm) in the interaction region with the laser, 150 cm downstream from the nozzle. In the imaging chamber, the state-selected molecular beam of OCS molecules is intersected at right angles by a linearly polarized photolysis laser at 230 nm. The polarization of the photolysis laser is perpendicular to the propagation direction of the molecular beam. This laser also ionizes the nascent CO $(X^1\Sigma^+;v=0|J)$ photofragments, using a $(2+1)$ REMPI scheme via two-photon Q-band transitions to the $B^1\Sigma^+$ resonant intermediate state.[20] The produced photofragment ions are velocity mapped[26] onto a position sensitive microchannel-plate (MCP)/phosphorscreen detector. A photomuliplier is used to collect the light of the mass-gated MCP/phosphorscreen to measure the total ion yield.[9] A CCD camera records simultaneously the spatial intensity distribution of the light from the phosphorscreen.

III. RESULTS

The hexapole focusing curve is shown in Fig. 2. The total yield of S $(^1D_2)$ fragments from photolysis of OCS at 230 nm was measured by a second laser at 291.48 nm using $(2+1)$ REMPI of S $(^1D_2)$ via the two-photon resonant $^1P_1$ intermediate state. The two peaks at voltages of 2.8 and 4.2 kV correspond to OCS parent molecules in the vibrationally excited $(\nu_2=1|JlM=111)$ and $(\nu_2=1|JlM=212)$ states, respectively. At a voltage of 8 kV a strong (broad) peak is observed, which can be assigned to molecules in the $(\nu_2=0|JM=10)$ vibrational ground state focusing by a second-order Stark effect.[23] Underlying the broad peak are also contributions from molecules in $(\nu_2=1|JlM)$ states with a lower effective dipole moment (see below and Sec. IV). In the experiments reported here the hexapole was set at either
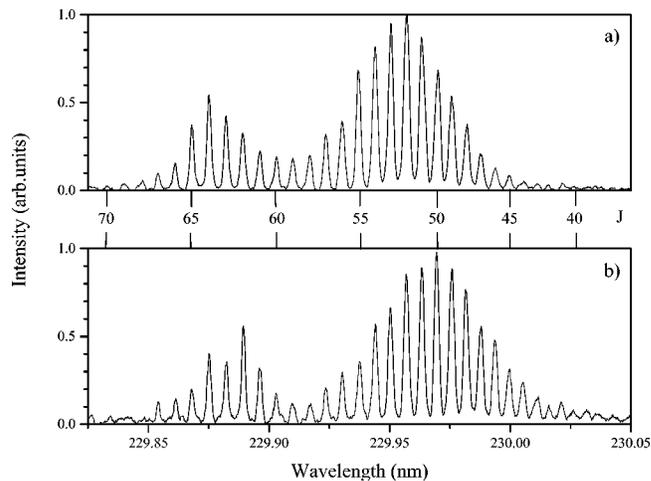

FIG. 3. Rotational $(2+1)$ REMPI spectra of the $\Delta v=0$, Q branch of the $B^1\Sigma^+\leftarrow\leftarrow X^1\Sigma^+$ transition of CO. The spectrum in panel (a) is for the dissociation of OCS with the hexapole at 2.8 kV, at which voltage OCS selected in a single quantum state $(\nu_2=1|JlM=111)$ are focused in the laser interaction region. The spectrum in panel (b) is for the dissociation of OCS with the hexapole at 8.0 kV, at which voltage both ground state OCS molecules $(\nu_2=0|JM=10)$ as well as several other vibrationally excited OCS molecules $(\nu_2=1|JlM)$ are focused in the laser interaction region. In the middle the assigned CO rotational levels J are indicated. Note how the maxima of the bimodal distribution in the spectrum in (a) are shifted about two quanta relative to the maxima in spectrum in (b). The REMPI spectra are combined with the 2-D images to extract the true populations of the individual J states for the dissociation of OCS molecules in the single quantum states $(\nu_2=0|JM=10)$ and $(\nu_2=1|JlM=111)$ (see Table I and Sec. III).

2.8 or 8.0 kV, to dissociate state-selected OCS molecules in the $(\nu_2=1|JlM=111)$ and $(\nu_2=0|JM=10)$ states, respectively.

The CO $(X^1\Sigma^+;v=0|J)$ rotational state distribution was deduced from spectra recorded by scanning the laser over the wavelength range 229.80–230.05 nm. Such spectra were taken for both OCS parent molecules with the hexapole set at 2.8 kV, state selecting OCS $(\nu_2=1|JlM=111)$, and at 8.0 kV, state selecting OCS $(\nu_2=0|JM=10)$. The CO rotational spectra are shown in Fig. 3. The bimodal structure in the rotational distribution, which was reported before for dissociation of non-state-selected molecules,[11,17,20–22] is clearly observed.

We see that the spectrum for the dissociation of OCS $(\nu_2=0|JM=10)$ cuts off at $J\geqslant68$ (see Fig. 3). This is at remarkably lower J levels than was observed in the photoelectron study of Rijs et al.,[22] where CO $(X^1\Sigma^+;v=0|J)$ could be detected and assigned for rotational levels up to $J=87$. In this latter experiment an effusive expansion of OCS was used, and the rotational spectrum reported in Fig. 1 of Ref. 22 shows a tail of rotational peaks $J=68$–87. This high-J tail of the rotational distribution is most likely due to photodissociation of vibrationally excited OCS $(\nu_2=1,2)$ parent molecules. Although these excited bending levels of OCS are much less populated than the ground state of OCS at 300 K, the strong increase of the transition dipole moment with a bending angle will enhance the absorption cross section substantially.[11]

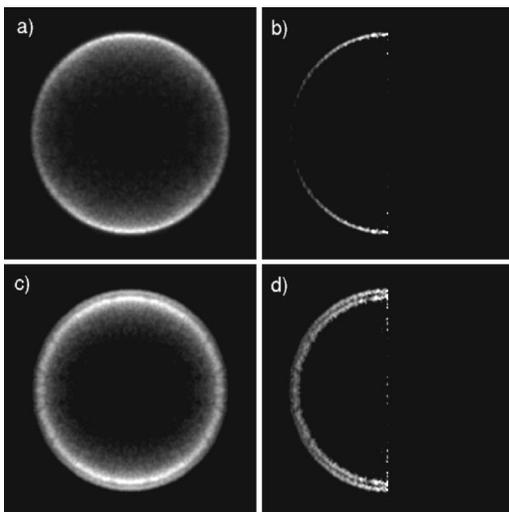For each of the rotational lines of CO, $J=43$–67, ion

FIG. 4. (a) Raw data image of the 2-D projected recoil distribution of the CO ($X\,^1\Sigma^+; v = 0 | J = 52$) photofragment, after the photodissociation of state-selected OCS with the hexapole voltage set at 2.8 kV. The hexapole state selector focuses OCS molecules in a single quantum-state ($\nu_2 = 1 | JlM = 111$). (b) The Abel-inverted image of data in (a) showing a 3-D cut of the recoil distribution of CO ($X\,^1\Sigma^+; v = 0 | J = 52$), Note that this cut is cylindrically symmetric around the vertical direction of the polarization of the laser. A single narrow velocity ring is observed. Both images are 312 by 312 pixels. (c) The same as (a), but with the hexapole set at 8.0 kV. This hexapole voltage focuses both ground state OCS molecules ($\nu_2 = 0 | JM = 10$), leading to slower CO fragments in the inner ring, and vibrationally excited OCS molecules ($\nu_2 = 1 | JlM$), leading to faster CO photofragments in the outer ring. (d) The Abel-inverted 3-D cut of data in (c). A different angular distribution can be observed for the outer and inner ring; the inner ring has more intensity to larger polar angles toward 90°, indicating a more isotropic angular distribution than the outer ring.

images were recorded while state selecting OCS ($\nu_2 = 0 | JM = 10$) or ($\nu_2 = 1 | JlM = 111$). During these measurement the Doppler profile of each line is scanned while the CCD camera is collecting the signal. The acquisition time for each image was typically 10 min, which corresponds to an accumulation of 6000 laser shots. The laser energy was 1.5 mJ/pulse. To prevent broadening and overlap of the lines in the rotational spectrum the laser beam was focused (with a lens with focal length of 20 cm) about 2 cm before the crossing with the state-selected molecular beam.

A typical data image of the CO ($X\,^1\Sigma^+; v = 0 | J = 52$) photofragment after photolysis of OCS with the hexapole set at 2.8 kV is shown in Fig. 4(a), and with the hexapole set at 8.0 kV in Fig. 4(c). Because the Q band of the (2+1) REMPI transition is not sensitive to alignment of the CO (J) fragment,[20] the obtained images are Abel invertible (also see Sec. IV). The Abel-inverted images of the 2-D data of Figs. 4(a) and 4(c) are shown in Figs. 4(b) and 4(d), respectively. Only half of the 3-D cut is shown as it is cylindrically symmetric about the vertical axis of the laser polarization. As can be seen in Figs. 4(c), 4(d) two closely spaced rings are observed when we set the hexapole at 8.0 kV. From a calculation of the energy available to the photofragments and the calibration of our velocity map ion lens, we can conclude that the inner ring correlates to photodissociation of the OCS ($\nu_2 = 0 | JM = 10$) state. The outer ring orginates from dissociation of several OCS ($\nu_2 = 1 | JlM$) excited states that
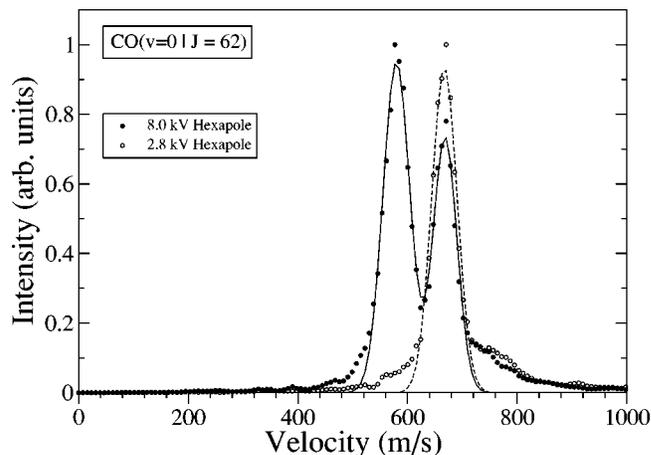

FIG. 5. Velocity distribution of the CO ($J = 62$) photofragments from the photodissociation of OCS parent molecules selected with the hexapole at 2.8 and 8.0 kV. The intensities of both distributions are scaled to unity. The two peaks in the distribution at 8.0 kV are well separated and the velocity difference corresponds to the energy difference between OCS ($\nu_1, \nu_2, \nu_3 = 0,0,0$) and OCS ($\nu_1, \nu_2, \nu_3 = 0,1^1,0$), i.e., 520.4 cm^{-1}.[17] The curves through the data points are fitted Gaussian-shaped functions. From the fitted intensities we deduce the relative contribution of the vibrationally excited OCS molecules focused at 8.0 kV. We subtract this contribution from the line intensities of the REMPI spectrum (see Fig. 3) to obtain the true rotational state population from the photodissociation of OCS($\nu_2 = 0 | JM = 10$), as given in Table I.

underlie the broad peak at 8.0 kV in the focusing spectrum (see Fig. 2). Multiple rings were never observed when the hexapole was set at 2.8 kV [see Figs. 4(a) and 4(b)], which is a clear experimental prove of the single ($\nu_2 = 1 | JlM = 111$) state of OCS selected at this hexapole voltage.

From the Abel-inverted images we can extract directly the velocity distribution of the CO ($X\,^1\Sigma^+; v = 0 | J$) fragment. In Fig. 5 we show the velocity distribution of CO ($X\,^1\Sigma^+; v = 0 | J = 62$) from the photodissociation of OCS with the hexapole set at the two voltages of 2.8 and 8.0 kV. When the hexapole is set at 2.8 kV only a single peak is observed in the velocity distribution, CO ($X\,^1\Sigma^+; v = 0 | J = 62$) from dissociation of OCS ($\nu_2 = 1 | JlM = 111$). The dashed line in Fig. 5 gives a Gaussian-shaped fit to the experimental velocity distribution. When the hexapole is set at 8.0 kV, two peaks are observed in the velocity distribution. The solid line in Fig. 5 gives a fit to the experimental velocity distribution of a superposition of two Gaussian-shaped functions. In this latter experiment the initial and final rovibrational quantum states of the OCS parent molecule and the CO ($X\,^1\Sigma^+; v = 0 | J = 62$) fragment molecule are specified. The OCS ($\nu_2 = 1 | JlM = 211$) or ($\nu_2 = 1 | JlM = 312$) states focus, due to the linear Stark effect, at hexapole voltages of 8.4 kV, a factor of 3 larger than the voltage of the ($\nu_2 = 1 | JlM = 111$) state [effective permanent dipole moment scales with $Ml/J(J+1)$]. This means that the difference in available energy between the selected OCS molecules around 8.0 kV must be completely released into translational energy of the CO ($X\,^1\Sigma^+; v = 0 | J = 62$) fragment molecule. Therefore, neglecting the very small rotational energy difference between OCS ($\nu_2 = 0 | JM = 10$) and OCS ($\nu_2 = 1 | JlM = 211,312$), we know that the velocity difference between

TABLE I. Rotational state population and β parameter of CO$(X\,^1\Sigma^+;v=0|J)$ from the dissociation of single state-selected OCS$(\nu_2=0|JM=10)$ and OCS$(\nu_2=1|JlM=111)$ at 230 nm. The error in β represents the standard deviation of the average β extracted from three independent measurements.

CO(J)	OCS$(\nu_2=0|JM=10)$ population	β	OCS$(\nu_2=1|JlM=111)$ population	β
43	0.20	0.61 ± 0.12	$\ldots$[a]	0.23 ± 0.05
44	0.31	0.61 ± 0.04	0.05	0.41 ± 0.08
45	0.41	0.70 ± 0.03	0.09	0.60 ± 0.02
46	0.58	0.37 ± 0.05	0.13	0.51 ± 0.02
47	0.64	0.38 ± 0.04	0.21	0.53 ± 0.02
48	0.91	0.25 ± 0.02	0.34	0.57 ± 0.01
49	0.96	0.19 ± 0.03	0.50	0.69 ± 0.03
50	1.0	0.17 ± 0.02	0.63	0.65 ± 0.04
51	0.96	0.13 ± 0.03	0.85	0.70 ± 0.02
52	0.69	0.25 ± 0.03	1.0	0.63 ± 0.02
53	0.44	0.29 ± 0.05	0.9	0.75 ± 0.01
54	0.32	0.49 ± 0.09	0.8	0.76 ± 0.01
55	0.12	0.47 ± 0.05	0.75	0.95 ± 0.05
56	0.12	0.92 ± 0.07	0.4	0.95 ± 0.04
57	0.06	0.95 ± 0.08	0.33	1.13 ± 0.03
58	0.03	1.41 ± 0.07	0.2	1.23 ± 0.05
59	0.08	1.51 ± 0.09	0.2	1.61 ± 0.03
60	0.12	1.69 ± 0.05	0.2	1.66 ± 0.03
61	0.25	1.65 ± 0.04	0.25	1.81 ± 0.04
62	0.61	1.75 ± 0.04	0.35	1.84 ± 0.02
63	0.36	1.50 ± 0.10	0.45	1.75 ± 0.03
64	0.28	1.64 ± 0.01	0.60	1.69 ± 0.02
65	0.19	1.42 ± 0.01	0.45	1.71 ± 0.05
66	0.05	1.17 ± 0.08	0.16	1.63 ± 0.01
67	0.05	0.98 ± 0.05	0.1	1.59 ± 0.02
68	$\ldots$[a]	$\ldots$[a]	0.07	$\ldots$
69	$\ldots$[a]	$\ldots$[a]	0.04	$\ldots$

[a]No analysis due to very low or absent signal.

the rings corresponds to the difference in the available energy from dissociation of the linear, $\nu_2=0$, and the bent, $\nu_2=1$, parent molecule, 520.4 cm^{-1}.[29] This provides a direct calibration of our velocity imaging detector.

The velocity we obtain for CO$(X\,^1\Sigma^+;v=0|J=62)$ in OCS$(\nu_2=0|JM=10)$ is used to extract an accurate dissociation energy D_0 of OCS$(\nu_1,\nu_2,\nu_3=0,0,0|J=0)\rightarrow$CO$(X\,^1\Sigma^+;v=0|J=0)+S(^1D_2)$. With the vacuum one-photon energy for (2+1) REMPI detection of CO$(X\,^1\Sigma^+;v=0|J=62)$ reported recently,[22] $\tilde{\nu}=43\,503.3$ cm^{-1}, the rotational energy E_{rot}CO$(X\,^1\Sigma^+;v=0|J=62)=7508.37$ cm^{-1}, E_{kin}CO$(J=62)=(1447\pm72)$ cm^{-1} from the image, E_{rot}OCS$(\nu_2=0|J=1)=0.4057$ cm^{-1} we obtain, $D_0=43\,503.3-7508.37-1447(72)+0.4057=(34549\pm72)cm^{-1}=(4.284\pm0.009)$eV. The previously reported experimental value was $D_0=4.26$ eV,[30] about 0.02 eV lower than the new value obtained here.

In Table I we give the rotational population extracted from the spectra given in Fig. 3. Because the spectrum obtained at 8.0 kV contains contributions from both the dissociation of OCS$(\nu_2=0|JM=10)$ and the dissociation of vibrationally excited OCS$(\nu_2=1|JlM)$ states, we have used the images measured at each rotational state to correct for the excited state contribution. The velocity distribution extracted from each Abel-inverted CO(J) image was used to integrate both the slow speed, n_{slow}, and the high speed component n_{fast}; see, e.g., Fig. 5. The peak intensity of the rotational line J in the spectrum (b) of Fig. 3 was then multiplied by $n_{\text{slow}}/(n_{\text{slow}}+n_{\text{fast}})$ to obtain the true CO(J) populations for dissociation of OCS$(\nu_2=0|JM=10)$ (see Table I).

The rotational spectra of photolysis of state-selected parent molecules show that for the bent molecule, the CO photofragment distribution shifts to higher J states. The maximum peak in the fast channel shifts from $J=50$ to $J=52$, in the slow channel from $J=62$ to $J=64$. Using the rotational constants of CO$(X\,^1\Sigma^+;v=0)$ (see, e.g., Table 1 in Ref. 22) and the rotational populations of Table I we can calculate the average rotational energy in the fast $(J=41-55)$ and slow $(J=60-65)$ channels. We find $\langle E_{\text{rot,fast}}(JM=00)\rangle=4710$ cm^{-1}, $\langle E_{\text{rot,fast}}(JlM=111)\rangle=5230$ cm^{-1}, $\langle E_{\text{rot,slow}}(JM=00)\rangle=7640$ cm^{-1}, and $\langle E_{\text{rot,slow}}(JlM=111)\rangle=7760$ cm^{-1}. It appears that in the fast channel all the additional initial OCS bending energy of 520.4 cm^{-1} is released in rotational energy. In the high J channel the average rotational energy from dissociation of the ground state or bent OCS is very similar, and (most of) the additional energy appears to be released into translational energy.

From the Abel-inverted images of the CO(J) photofragments, the anisotropy of the angular distribution was calculated. The anisotropy parameter β was extracted by projecting the second Legendre coefficient from the angular distribution [see Eq. (2)].

The β parameter for each CO(J) level is depicted in Fig. 6. The error bars indicate the average over three independent measurements. As can be seen, the rotationally cold
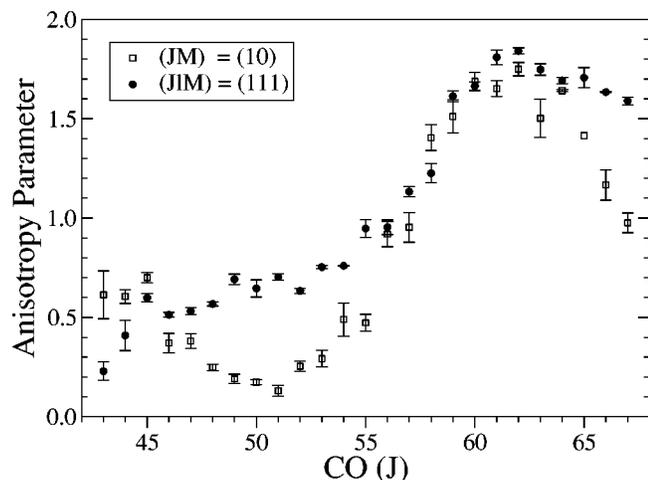
FIG. 6. The anisotropy β parameter as a function of the CO rotational quantum number, J, for the dissociation of OCS($\nu_2=0|JM=10$) (open squares) and OCS ($\nu_2=1|JlM=111$) (solid circles). The error bars indicate one standard deviation of the statistical average of three independent measurements.

CO channel ($J=41–55$) has a relatively low β value. These rotational levels correspond to CO fragments with high velocity. The levels $J=60–65$ correspond to the hot channel in the CO rotational distribution with a slow velocity. For these levels a relatively high β parameter, close to the maximum of two, is observed. Furthermore, especially for the rotationally cold channel, a higher β value for the bent molecule ($\nu_2=1|JlM=111$) than for the linear molecule ($\nu_2=0|JM=10$) was found for $J=46–53$.

IV. DISCUSSION

A. M-state selection and the β parameter

In the extraction of the β parameter (see Sec. III), we assumed that the 2-D images were Abel invertible. At this point we would like to address this assumption in more detail. The state-selected OCS ($\nu_2=1|JlM=111$) molecules, after passing through the hexapole and a field-free region,[2] enter the extraction region in the electrostatic velocity map lens. The M quantum number indicates the projection of the total angular momentum J on an external axis, so a nonzero value implies spatial orientation of the parent molecule. Because of the absence of nuclear spin in all the atoms in OCS, the state-selected OCS ($\nu_2=1|JlM=111$) wave function will be very well conserved also in the absence of electric fields. The Stark-curves do not intersect and when the state-selected molecules enter the ion-lens region, they will feel the electric field between the extraction electrodes. Consequently, the OCS ($\nu_2=1|JlM=111$) will be oriented in the extraction region of the electrostatic lens before dissociation. Using the expression derived for the saturation, S, of the uncoupling of the l doubling of the ($JlM=111$) wave function,[31] we find that for an electric field of ≈ 68 V/cm (this is the field strength in the middle between our repeller and extractor), $S=0.883$ for OCS.[24] This means that the ($\nu_2=1|JlM=111$) wave function is almost completely oriented, $\langle\cos(\vec{E}_{\text{extract}},\vec{d})\rangle=0.44$ (maximum value$=0.5$). Here

$\vec{E}_{\text{extract}}$ is the ion extraction electric field and $\vec{d}$ the permanent dipole moment of OCS. It follows that the ($\nu_2=1|JlM=111$) state is oriented along the propagation direction of the molecular beam (and the TOF axis), with the sulfur side of the molecule pointing toward the positive repeller electrode. The bond orientation along the TOF axis breaks the cylindrical symmetry of the experiment about the photolysis polarization direction. In principle, the Abel inversion cannot be rigorously applied in such a situation. However, an analysis of a forward-projected single-speed spatial distribution containing the ($\nu_2=1|JlM=111$) angular distribution along the TOF axis, shows that this broken symmetry does not significantly affect the value of the observed anisotropy parameter β. Furthermore, a direct measurement of the angular distribution of the outer ring of experimental two-dimensional projected CO images give the same β parameter as the angular distribution from the three-dimensional Abel-inverted images. We believe that this particular symmetry breaking can affect the speed distribution only and not the angular distribution, and since the speed distributions in these experiments are unambiguous (they are delta functions), use of the Abel transform does not cause any systematic error.

The laboratory frame spatial orientation probability of the OCS bond axis about the direction of the orientation field (which is along the time-of-flight axis) is given by $I(\theta_{\text{bond}})\sin\theta_{\text{bond}}d\theta_{\text{bond}}$, and the orientational density distribution, $I(\theta_{\text{bond}})$, can be described by an expansion of Legendre polynomials.[2,32] For a rotational state $J=1$, the expansion is terminated at the second Legendre polynomial:

$$I(\theta_{\text{bond}})=0.5+c_1P_1(\cos\theta_{\text{bond}})+c_2P_2(\cos\theta_{\text{bond}}),\quad(3)$$

where θ_{bond} is the laboratory frame angle between the OCS bond axis and the orientation field. The orientational distribution is normalized, c_1 describes the bond *orientation*, and c_2 the bond *alignment*. For the ($\nu_2=0|JM=10$) state, $c_1=0$ and $c_2=\frac{1}{4}$, i.e., only alignment of the bond axis but no orientation. For the ($\nu_2=1|JlM=111$) state, $c_1=\frac{3}{4}$ and $c_2=\frac{1}{4}$. Notice that these two states possess the same degree of bond alignment (about the TOF axis), whereas only the ($\nu_2=1|JlM=111$) state has a spatially oriented bond axis. In this latter case, because we focus positive Stark-effect states, the OCS bond axis is oriented along the time-of-flight axis with the sulfur side of the molecule toward the repeller plate and the oxygen side toward the extractor plate of the velocity map ion lens.

The angular recoil distribution of photofragments from oriented and aligned parent molecules has been calculated.[33,34] This angular distribution can be shown to depend on the angle α_d between the permanent dipole moment $\vec{d}$ and the recoil direction $\vec{v}$, and the angle χ between the transition dipole moment, $\vec{\mu}$, and the recoil direction. The laboratory frame angular distribution of photofragments about the photolysis polarization (which is at 90° to the direction of the orientation field and parallel to the detector plane) in a plane perpendicular to the orientation field (as in the current experimental geometry this plane is parallel to the MCP/CCD detector plane) is given by[33,34]

$$I(\theta) = 1 + \{(2P_2(\cos\chi) + \Delta)/(1-\Delta)\}P_2(\cos\theta), \quad (4a)$$

$$\Delta = \tfrac{3}{4}c_2 \sin^2\chi \sin^2\alpha_d/(1 + 2\,c_2 P_2(\cos\alpha_d)). \quad (4b)$$

Notice that the angular distribution depends only on the degree of parent molecule alignment (c_2), but not on the orientation. Therefore, both the ($\nu_2=0|JM=10$) and ($\nu_2=1|JlM=111$) states will be affected in the same way, $c_2 = \tfrac{1}{4}$, in both cases. For axial recoil, and for a pure parallel transition ($\chi=0$), Eq. (4) reduces to $[1+2P_2(\cos\theta)]$, whereas for a pure perpendicular transition ($\chi=\pi/2$), Eq. (4) reduces to $[1-P_2(\cos\theta)]$ (for all values of α_d), which are the usual limits for Eq. (1). Therefore, in the axial recoil limit, there is *no effect* of parent orientation or alignment on the photofragment angular distribution in the plane perpendicular to the orientation field. For the case of nonaxial recoil, it is well known that the angular distribution of the photofragments of unaligned parent molecules is given by[35,36]

$$I(\theta) = 1 + 2P_2(\cos\chi)P_2(\cos\theta). \quad (5)$$

For $c_2=0$ (i.e., unaligned parent molecules), or for $\alpha_d=0$ (i.e., $\vec{v}$ parallel to $\vec{d}$), Eq. (4) reduces to Eq. (5). Therefore, we see that for deviation from Eq. (5), we need χ, α_d, and c_2 to be nonzero.

In Sec. IV B, we discuss the dependence of the direction of the parallel, A', component of the transition dipole moment with the molecular frame sulfur–CO vector. We find that for our bending wave functions this angle is initially around $\chi_{A'} \approx 16°$ or so. Now while the molecule starts dissociating and the S atom moves to even larger Jacobi angles (due to the strong anisotropy of the potential), the recoil velocity direction may even sweep through and pass beyond the initial direction of the transition dipole moment. This may lead still to rather small ($\approx 16°$) final angles χ needed to provide relatively large β parameters of 1.7–1.8. If we now take a value of $\chi \approx 16°$ and $\alpha_d=90°$ (to make the correction term Δ in Eq. (4a) maximum, though we expect realistic values of α_d to be about 40°), we find $\beta_{real}=1.77$ [Eq. (5)] and $\beta_{exp}=1.83$ [Eq. (4)]. We conclude from careful inspection of Eq. (4) that for our initial M-state-selected OCS parent molecules, for parallel transitions ($\vec{\mu}$ in the plane of the bent molecule) deviations of the experimentally observed β parameter from the true β parameter are generally very small (1%–3%), and for perpendicular transitions there are no deviations. The experimental β parameters reported in Table I and Fig. 6, for the two selected states, are therefore believed to represent the true β parameters, within our estimated experimental error.

We conclude that in this experimental geometry with the photolysis polarization perpendicular to the orientation field, the effect of parent orientation and alignment is negligible on the observed photofragment angular recoil distribution. However, these effects can become very large in other experimental geometries, which can be used to measure directly the angles of the recoil velocity with the transition dipole moment and the permanent dipole moment.[34]
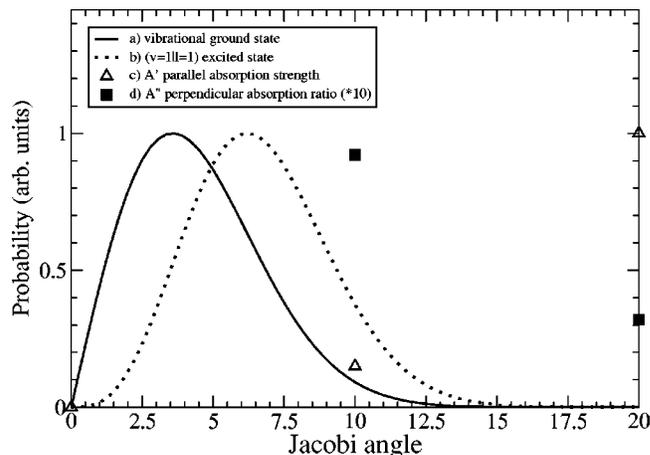

FIG. 7. The probability of the OCS ($\nu_2=0|JM=10$) ground state wave function, curve (a), and the OCS ($\nu_2=1|JlM=111$) vibrationally excited wave function, curve (b), versus Jacobi scattering angle θ_{Jacobi}, $|\psi(\theta_{Jacobi})|^2 \sin\theta_{Jacobi}$. The probability was calculated using the two-dimensional harmonic oscillator wave functions, with the following OCS parameters: interatomic distances $r_{CO}=2.194$ a.u., $r_{CS}=2.95$ a.u., $r_{CO-S}=4.204$ a.u., $\omega_{bend}=527$ cm^{-1}, $\kappa=7.952$, and $\eta=0.702$ (Ref. 35). Included are also the square of the parallel transition dipole moment, $|\vec{\mu}_{2\,^1A'}|^2$, curve (c), and the fraction (multiplied by ten) of the perpendicular transition probability $f_{perp}=|\vec{\mu}_{y,1\,^1A''}|^2/(|\vec{\mu}_{x,2\,^1A'}|^2+|\vec{\mu}_{y,1\,^1A''}|^2+|\vec{\mu}_{z,2\,^1A'}|^2)$, curve (d), as reported in Ref. 11.

B. Bending state selection and the β parameter

Suzuki and co-workers attributed the bimodal rotational state distribution of CO (J) to two processes.[11] The high-J channel was attributed to a process where OCS molecules are initially excited via a parallel transition to the $2\,^1A'$ surface and cross in the exit region to the ground state $1\,^1A'$ surface. This results in an angular distribution of CO (high J) originating from a purely parallel transition. In Fig. 6, in the region $J \approx 60-62$ we observe $\beta_{(10)} \approx 1.5-1.7$ and $\beta_{(111)} \approx 1.7-1.8$. It means we find β values close to but slightly lower than the limiting value of 2.0 for a purely parallel transition.

The data suggest that in this $J \approx 60-62$ region $\beta_{(10)}$ may be slightly lower than $\beta_{(111)}$. We have tried to reconcile these results in view of the calculated transition dipole moment function, as reported in Ref. 11. In Fig. 7 we plot the ($\nu_2=0$) and ($\nu_2=1|l=1$) two-dimensional isotropic harmonic-oscillator bending wave functions[35] as a function of the Jacobi angle, θ_{Jacobi}, which is the angle between the CO axis and the vector connecting the sulfur atom with the center-of-mass of CO. Unfortunately, the dipole moment function was calculated at intervals of 10° in the Jacobi angle only,[37] whereas the most interesting region for our state-selected experiments is the region 0°–20°. This means that we have limited information only on the Jacobi angle dependence. Still we believe we can extract a meaningful qualitative trend from the calculations. In Fig. 7 we added the electronic part of the absorption strength of the parallel transition, the transition dipole moment $|\vec{\mu}_{x,2\,^1A'}|^2 + |\vec{\mu}_{z,2\,^1A'}|^2$, at $\theta_{Jacobi}=0°$, 10°, and 20°. As can be observed, the parallel transition strength strongly increases with increasing bending angle. Furthermore, from the μ_x and μ_z components of the transition dipole moment[37] (which are in

the plane of the bending molecule and thus have A' symmetry) we can calculate the angle, $\chi_{A'} = \mathrm{atan}(\mu_x/\mu_z)$, between the parallel transition dipole moment, $\vec{\mu}_{2\,^1A'} = \vec{\mu}_x + \vec{\mu}_z$ and the recoil velocity $\vec{v}_S$. We find $\chi_{A'} = 16°$ at $\theta_{\mathrm{Jacobi}} = 10°$, and $\chi_{A'} = 7°$ at $\theta_{\mathrm{Jacobi}} = 20°$, it means $\chi_{A'}$ decreases somewhat with increasing Jacobi angle. As can be seen from Eq. (5), for large β parameters (≈ 1.7–2.0), the magnitude of β is mainly determined by the magnitude of $2P_2(\cos\chi)$, and decreases with increasing χ. From Fig. 7 we see that the excited bending wave function ($\nu_2 = 1|l = 1$) has a larger probability toward a larger Jacobi angle. In combination with the increasing parallel absorption strength, it means that smaller angles $\chi_{A'}$ contribute with increasing bending angle, which will result in a somewhat larger β parameter for the excited ($\nu_2 = 1|l = 1$) state compared to the ($\nu_2 = 0$) state, as we observe experimentally.

We will now address the region of low $J \approx 46$–55, which was attributed by Suzuki and co-workers[11] as resulting from a second process, a simultaneous absorption to the $2\,^1A'$ and $1\,^1A''$ surfaces with subsequent dynamics on these anisotropic surfaces leading to lower rotational excitation of CO (J). Also plotted in Fig. 7 at $\theta_{\mathrm{Jacobi}} = 10°$, $20°$ is the theoretically calculated[37] fraction of perpendicular transition strength, $f_{\mathrm{perp}} = |\vec{\mu}_{y,1\,^1A''}|^2/(|\vec{\mu}_{x,2\,^1A'}|^2 + |\vec{\mu}_{y,1\,^1A''}|^2 + |\vec{\mu}_{z,2\,^1A'}|^2)$ (note that the values are multiplied by 10 to be viewed well). It is seen that the perpendicular component of the transition dipole moment decreases with an increasing bending angle. Suzuki and co-workers[11] state that the CO (low-J) channel results from a simultaneous excitation to both the $1\,^1A''$ perpendicular and the $2\,^1A'$ parallel surfaces. We observe in Fig. 6 around the peak of the J distribution, $J \approx 51$, that $\beta_{(111)} = 0.70$ and $\beta_{(10)} = 0.13$. We see that the initial OCS parent state has a profound influence on the angular recoil distribution. Because of the larger amplitude of the OCS ($\nu_2 = 1|l = 1$) bending wave function at larger Jacobi angles, this results in a smaller contribution of the perpendicular component and thus a larger $\beta_{(111)}$, relative to $\beta_{(10)}$. If we assume that the β parameter for the parallel transition, $\beta_{A'} = 1.8$, and for the perpendicular transition $\beta_{A''} = -1.0$, we find from the experimental $\beta_{(10)}(J = 51) = 0.13$, $f_{\mathrm{perp}}(10) = 0.6$, and from $\beta_{(111)}(J = 51) = 0.70$, from $f_{\mathrm{perp}}(111) = 0.39$. However, these values are much larger than a simple calculation of the quantity f_{perp} from the theoretical calculations of the transition dipole moment. This may be due to the Franck–Condon overlap of the bending wave functions in the electronic ground state and the wave function in the excited states, $2\,^1A'$ and $1\,^1A''$.

We observe for the dissociation of both initial OCS quantum states a general trend of an increasing β parameter with increasing CO (J), especially for $51 < J < 62$. This is in agreement with the measurements of Kim *et al.*[12] for the photodissociation of non-state-selected OCS at 223 nm. They find at low $J \approx 51$, $\beta = 0.35$, and at high $J \approx 65$, $\beta = 1.80$. Sato *et al.*[20] reported values $\beta = 0.6$ ($J = 47$) increasing to $\beta = 1.7$ ($J = 60$) for dissociation at 230 nm and non-state-selected OCS.

Recently, Sugita *et al.*[17] reported measurements of photodissociation of OCS at 230 nm. They reported β parameters from imaging experiments analyzing double rings in

TABLE II. Averaged anisotropy β parameter as observed for the rotationally cold and hot channel, for both the linear and bent OCS parent molecule. The values are obtained by averaging of the individual $\beta(J)$ parameters, as listed in Table I. The cold (translationally fast) and hot (translationally slow) channels were taken as the regions $J = 44$–55, and $J = 60$–65, respectively.

$\langle\beta\rangle$	OCS ($\nu_2 = 0|JM = 10$)	OCS ($\nu_2 = 1|JlM = 111$)
Cold (low J), fast channel	0.24	0.71
Hot (high J), slow channel	1.65	1.74

the images observed for CO (J) states with $J = 65$–67. The β parameters obtained for dissociation of vibrationally excited OCS ($\nu_2 = 1$) for $J = 65$–66 are in very good agreement with our values, their $\beta (J = 67) = 1.2$ is somewhat lower than the value of 1.6 that we observe (see Fig. 6). The β parameters they report for the dissociation of vibrational ground state OCS ($\nu_2 = 0$) for $J = 63$–67 are about 0.2–0.5 lower than we observe.

For J states $J = 63$–67, the β parameter is decreasing with increasing J relative to the peak value of ≈ 1.7–1.8 at $J = 61$–62 (see Fig. 6). This may be due to a dynamical reduction of the observed β parameter caused by an increasing off-axis recoil at these very high rotational angular momenta.[35,38]

To compare our results with previous measurements of the β parameter obtained from measurements of the S $(^1D_2)$ recoil distribution for slow S fragments, correlating with rotationally hot CO (J), and fast S fragments, correlating with rotationally cold CO (J), we calculated a rotational state population weighted average of $\langle\beta_{\mathrm{slow}}\rangle$ (averaged over rotational states $60 \leq J \leq 65$) and $\langle\beta_{\mathrm{fast}}\rangle$ (averaged over rotational states $46 \leq J \leq 55$). The results are given in Table II for the dissociation of OCS ($\nu_2 = 0|JM = 10$) and OCS ($\nu_2 = 1|JlM = 111$). These averaged β values, especially for OCS ($\nu_2 = 0|JM = 10$), are in good agreement with the values reported by Rakitzis *et al.*,[14] $\beta_{\mathrm{fast}} = (0.2 \pm 0.1)$ and $\beta_{\mathrm{slow}} = (1.4 \pm 0.2)$, for the dissociation of non-state-selected OCS at 223 nm. Suzuki and co-workers reported[11] $\beta_{\mathrm{fast}} = 0.7$ and $\beta_{\mathrm{slow}} = 1.8$ under similar experimental conditions at 223 nm. This similarity in β parameters between dissociation at 223 and 230 nm suggests that the dynamics reflected by the β parameter does not change very much in the wavelength region 223–230 nm.

To summarize, our measured β parameters and rotational state populations of recoiling CO (J) for the dissociation of single state-selected OCS ($\nu_2 = 0|JM = 10$) and OCS ($\nu_2 = 1|JlM = 111$), provide very detailed information on the dissociation dynamics of OCS. It enables a good test of the theoretical calculations by Suzuki and co-workers,[11] especially regarding the bending-angle dependence of the transition dipole moment function. More detailed quantum state-to-state calculations on the *ab initio* excited state surfaces are needed to enable a rigorous comparison of our state-to-state experimental data.

V. CONCLUSIONS

We have reported the state-to-state resolved angular recoil distribution of $CO(X\,^1\Sigma^+;v=0|J)$ from the photodissociation of $OCS(\nu_2=0|JM=10)$ and $OCS(\nu_2=1|JlM=111)$. For the experimental geometry used here, the M-state selection has a negligible effect on the angular distribution and the extracted β parameter. The influence of the initial OCS bending motion on the photodissociation is quantified both in the rotational state distribution as the β parameter. When the parent molecule is in the first excited bending mode, the additional vibrational energy of OCS is completely released in rotational energy for the fast speed, low-J $CO(J)$ channel. For the slow speed, high-J $CO(J)$ channel, the average rotational energy of the CO fragment is very similar between the two initial OCS states. For the rotationally cold $CO(J)$ channel, a significant dependence of the anisotropy parameter β on the initial OCS bending state is found. Near the peak of the rotational state distribution, $J\approx51$, $\beta_{(10)}$ is smaller than $\beta_{(111)}$. This may result from a larger contribution of the perpendicular excitation to the $1\,^1A''$ surface for the dissociation of $OCS(\nu_2=0|JM=10)$ compared to the dissociation of $OCS(\nu_2=1|JlM=111)$. The state-to-state experiments allow an accurate determination of the binding energy of OCS.

In a future publication we will report on similar state-to-state experiments of OCS, but now detecting the $S(^1D_2)$ angular distribution. A series of experiments with varying polarizations of pump and probe laser enable measurements of the alignment and coherences in the $S(^1D_2)$ recoil distribution. These type of experiments provide unprecedented data to compare and test the quality of *ab initio* surfaces and (nonadiabatic) quantum dynamical calculations of the benchmark photodissociation system OCS.

[1] H. Sato, Chem. Rev. **101**, 2687 (2001).
[2] M. H. M. Janssen, J. W. G. Mastenbroek, and S. Stolte, J. Phys. Chem. A **101**, 7605 (1997).
[3] T. P. Rakitzis, S. A. Kandel, A. J. Alexander, Z. H. Kim, and R. N. Zare, Science **281**, 1346 (1998).
[4] T. P. Rakitzis, S. A. Kandel, A. J. Alexander, Z. H. Kim, and R. N. Zare, J. Chem. Phys. **110**, 3351 (1999).
[5] A. S. Bracker, E. R. Wouters, A. G. Suits, and O. S. Vasyutinskii, J. Chem. Phys. **110**, 6749 (1999).
[6] A. J. Alexander, Z. H. Kim, S. A. Kandel, R. N. Zare, T. P. Rakitzis, Y. Asano, and S. Yabushita, J. Chem. Phys. **113**, 9022 (2000).
[7] A. T. J. B. Eppink, D. H. Parker, M. H. M. Janssen, B. Buijsse, and W. J. van der Zande, J. Chem. Phys. **108**, 1305 (1998).
[8] D. W. Neyer, A. J. R. Heck, D. W. Chandler, J. M. Teule, and M. H. M. Janssen, J. Phys. Chem. A **103**, 10388 (1999).
[9] J. M. Teule, G. C. Groenenboom, D. W. Neyer, D. W. Chandler, and M. H. M. Janssen, Chem. Phys. Lett. **320**, 177 (2000).
[10] M. Ahmed, E. R. Wouters, D. S. Peterka, O. S. Vasyutinskii, and A. G. Suits, Faraday Discuss. **113**, 425 (1999).
[11] T. Suzuki, H. Katayanagi, S. Hanbu, and M. Aoyagi, J. Chem. Phys. **109**, 5778 (1998).
[12] Z. H. Kim, A. J. Alexander, and R. N. Zare, J. Phys. Chem. A **103**, 10144 (1999).
[13] T. P. Rakitzis, P. C. Samartzis, and T. N. Kitsopoulos, J. Chem. Phys. **111**, 10415 (1999).
[14] T. P. Rakitzis, P. C. Samartzis, and T. N. Kitsopoulos, Phys. Rev. Lett. **87**, 123001 (2001).
[15] S. M. Dylewski, J. D. Geiser, and P. L. Houston, J. Chem. Phys. **115**, 7460 (2001).
[16] J. W. G. Mastenbroek, C. A. Taatjes, K. Nauta, M. H. M. Janssen, and S. Stolte, J. Phys. Chem. **99**, 4360 (1995).
[17] A. Sugita, M. Mashino, M. Kawasaki, Y. Matsumi, R. Bersohn, G. Trott-Kriegeskorte, and K. Gericke, J. Chem. Phys. **112**, 7095 (2000).
[18] M. S. Johnson, G. D. Billing, A. Gruodis, and M. H. M. Janssen, J. Phys. Chem. A **105**, 8672 (2001).
[19] T. P. Rakitzis, Chem. Phys. Lett. **342**, 121 (2001).
[20] Y. Sato, Y. Matsumi, M. Kawasaki, K. Tsukiyama, and R. Bersohn, J. Phys. Chem. **99**, 16307 (1995).
[21] N. Sivakumar, G. E. Hall, P. L. Houston, J. W. Hepburn, and I. Burak, J. Chem. Phys. **88**, 3692 (1988).
[22] A. M. Rijs, E. H. G. Backus, C. A. de Lange, M. H. M. Janssen, N. P. C. Westwood, K. Wang, and V. McKoy, J. Chem. Phys. **116**, 2776 (2002).
[23] S. R. Gandhi and R. N. Bernstein, J. Chem. Phys. **87**, 6457 (1987).
[24] J. M. L. J. Reinartz, W. L. Meerts, and A. Dynamus, Chem. Phys. Lett. **116**, 576 (1972).
[25] H. Jalink, F. Harren, D. van den Ende, and S. Stolte, Chem. Phys. **108**, 391 (1986).
[26] A. T. J. B. Eppink and D. H. Parker, Rev. Sci. Instrum. **68**, 3477 (1997).
[27] F. Harren, D. H. Parker, and S. Stolte, Comments At. Mol. Phys. **26**, 109 (1991).
[28] R. W. Anderson, J. Phys. Chem. A **101**, 7664 (1997).
[29] Y. Morino and T. Nakagawa, J. Mol. Spectrosc. **26**, 496 (1968).
[30] W. L. Weise, M. W. Smith, and B. M. Miles, Natl. Stand. Ref. Data Ser. **22**, 134 (1969).
[31] C. H. Townes and A. L. Shawlow, in *Microwave Spectroscopy* (McGraw-Hill, New York, 1955).
[32] S. E. Choi and R. B. Bernstein, J. Chem. Phys. **85**, 150 (1986).
[33] C. A. Taatjes, M. H. M. Janssen, and S. Stolte, Chem. Phys. Lett. **203**, 363 (1993).
[34] T. P. Rakitzis, A. J. van den Brom, and M. H. M. Janssen (in preparation).
[35] M. D. Morse and K. F. Freed, J. Chem. Phys. **74**, 4395 (1981).
[36] G. E. Bush and K. R. Wilson, J. Chem. Phys. **56**, 3638 (1972).
[37] T. Suzuki (private communication).
[38] D. W. Neyer, A. J. R. Heck, and D. W. Chandler, J. Chem. Phys. **110**, 3411 (1999).